Assessment of IASI capability for retrieving Carbonyl Sulphide (OCS)

C. Camy-Peyret, G. Liuzzi, G. Masiello, C. Serio, S. Venafra, S.A. Montzka

PII: S0022-4073(17)30248-0
DOI: 10.1016/j.jqsrt.2017.07.006
Reference: JQSRT 5773

To appear in: *Journal of Quantitative Spectroscopy & Radiative Transfer*

Received date: 24 March 2017
Revised date: 8 July 2017
Accepted date: 10 July 2017

Please cite this article as: C. Camy-Peyret, G. Liuzzi, G. Masiello, C. Serio, S. Venafra, S.A. Montzka, Assessment of IASI capability for retrieving Carbonyl Sulphide (OCS), *Journal of Quantitative Spectroscopy & Radiative Transfer* (2017), doi: 10.1016/j.jqsrt.2017.07.006

Highlights

- Among the first works showing Carbonyl sulphide (OCS) retrievals from IASI
- Case study based on two years long record of IASI soundings
- Comparison with in situ and airborne OCS observations

Assessment of IASI capability for retrieving Carbonyl Sulphide (OCS).

C. Camy-Peyret[a], G. Liuzzi[b], G. Masiello[b], C. Serio[b,*], S. Venafra[b] and and S.A. Montzka[c]

[b] *Institut Pierre-Simon Laplace (IPSL), UPMC/UVSQ, Paris, France*
[b] *Scuola di Ingegneria, Universitá della Basilicata, Potenza, Italy*
[c] *NOAA Earth System Research Laboratory, Boulder, Colorado, USA*

Abstract

The capability of IASI (Infrared Atmospheric Sounder Interferometer) for retrieving OCS has been assessed with a series of retrieval experiments, which have been carried out with a physical forward/inverse scheme, which can exploit the full IASI information content. We use random projections to reduce the dimensionality of the data space and to have a unified treatment of instrument and forward model errors. The OCS column amount is retrieved both by using a scaling parameterization of the profile and a non-parametric approach, in which we first derive the OCS profile and then its global amount is estimated by a proper integration over the profile. IASI OCS retrievals are compared to in situ flask observations at the Mauna Loa validation station, Hawaii, USA and observations from HIAPER Pole-to-Pole flights. We have found that the best way to retrieve OCS is through the non-parametric approach, which shows that the OCS cycle amplitude, phase and mean abundance can be retrieved with high accuracy for night and day time soundings. In fact, IASI captures the OCS seasonal cycle, with an overall difference with in situ observations, which is of the order of ≈ 1 pptv, provided we use HITRAN2012 OCS line compilation. HITRAN2008, which has been used in previous studies, is indeed affected by spectroscopic errors as far as OCS is concerned, which results in heavily biased

*C. Serio, carmine.serio@unibas.it

OCS retrievals. Although the present paper is mostly intended to assess IASI retrievals over ocean, a demonstrative application to above land surface is considered as well. Preliminary results suggest that IASI can recover the OCS cycle in ecosystems governed by leaf and/or soil sources/sinks.

Keywords: `Remote Sensing`, Infrared, Satellite, Spectroscopy, Forward Modelling, Carbon Cycle

1. Introduction

The importance of carbonyl (OCS) sulphide in the study of ecosystems has clearly emerged in recent studies [1, 2, 3, 4, 5, 6]. OCS is the most abundant sulphur-containing trace gas in the atmosphere, and carries a significant part of sulphur in the stratospheric aerosol [4]. Major sources of OCS are natural, and among them oceans, soils and volcanic eruptions play a dominant role. Otherwise, anthropogenic sources have been recognized as a secondary contributor: the most important of them are biomass burning and industrial activities [5]. The main sink of OCS has been identified as vegetation uptake, whose magnitude is also influenced by seasonal trends in vegetation growth. Conversely, in the stratosphere photochemical loss is the prominent process that removes OCS from the atmosphere. Moreover, OCS has recently emerged as a putative proxy for the photosynthetic uptake of CO_2, because OCS and CO_2 have the same diffusion pathway into leaves [1, 7], and OCS hydration reaction in this process is irreversible. The quantification of OCS concentration above forest canopy is also of primary interest to obtain indications about the direct impact of photosynthetic processes on the CO_2 seasonal and inter-annual trends. Therefore, the capability of IASI (Infrared Atmospheric Sounder Interferometer) for retrieving the seasonal cycle of OCS is an important asset. More recently, [3, 1, 8] have shown that OCS holds great promise for studies of carbon cycle processes because it is an atmospheric tracer of photosynthetic Gross Primary Production (GPP). According to [8, 9] the uptake of OCS from the atmosphere is dominated by the activity of carbonic anhydrase (CA), an enzyme abundant in leaves that

also catalyses CO_2 hydration during photosynthesis. However, as a continuation of previous studies, it has been shown in [7] (where previous references on this topic can be found) that soils also effectively exchange OCS with the atmosphere, which complicates the retrieval of GPP from atmospheric budgets. Agricultural fields can take up large amounts of OCS from the atmosphere as soil microorganisms also contain CA. In fact, OCS emissions from soils have been reported in agricultural elds or anoxic soils [10, 7]. These studies have urged satellite community to retrieve tropospheric OCS on a global scale. The first attempts have been performed with Aura Tropospheric Emission Spectrometer (TES) instrument [11, 12] and more recently with IASI [13, 14]. It is worth mentioning that OCS global distribution and hotspots have been also addressed with limb viewing instrumentation (e.g. [15, 16] and reference therein).

The present paper is aiming at complementing the above efforts and, possibly, improving our understanding about the reliability and capability of IASI observations to retrieve OCS over ocean and land. Although the paper is mainly intended to assess IASI retrieval accuracy for OCS over ocean, the study also presents an application to land surface. OCS IASI retrievals over the Po Valley (Italy) for the year 2015 have been considered. The Po Valley is characterized by intense farming and other intense activity linked to agriculture and therefore is an ecosystem where OCS sources and sinks are mainly governed by soil inflow/outflow.

In [12], authors estimated the column amount of OCS using a non-parametric approach, in which the OCS profile is first estimated and then the column amount is obtained through a proper integration. Conversely, [13, 14] used a parametric approach, in which a given reference OCS profile is parameterized with one scaling parameter. The retrieval is then performed by retrieving the scaling parameter. This last approach is expected to be good for gases such as CO_2, N_2O and CH_4, which have very long tropospheric lifetimes, therefore their climatological variability (usually inversely proportional to their tropospheric lifetimes) is expected to be very small and the vertical profile of its volume mixing ratio can be considered truly uniform, that is constant with altitude.

Initial estimates of the OCS tropospheric lifetime of 4-7 years [17] have been reviewed in [3] and are presently estimated to be 2-3 years. This is long enough to allow us to use a parameterization of a single uniform profile with a single scaling factor. In effect, the reference OCS profile from the AFGL climatology [18] is uniform through the troposphere with a constant value of about 510 pptv. However, airborne observations [3] have shown that OCS mixing ratios contain substantial vertical gradients that can vary with season and latitude, particularly over productive terrestrial ecosystems. Therefore, the quality and accuracy of the simple parametric approach has to be properly assessed against the non-parametric approach, a task that will be performed in this paper.

The retrieval analysis will be performed with a simultaneous physical retrieval approach [13], which uses all available observations of the IASI spectral coverage extending from 645 cm^{-1} to 2760 cm^{-1}. The retrieval scheme provides the simultaneous retrieval of all geophysical parameters, which are relevant to the formation of IASI spectra. These parameters include surface temperature and emissivity, temperature, water vapour, ozone, HDO, CO_2, CO, CH_4, SO_2, N_2O, HNO_3, NH_3, OCS and CF_4. The retrieval approach has been exemplified in [13] based on a case study, which consisted of a two year long record of IASI spectra over sea surface in the Pacific Ocean close to Mauna Loa (Hawaii) validation station, where surface-based samples are regularly collected and analysed for OCS [3]. An important, recent, improvement of the retrieval scheme consists in transforming the data space to one of reduced dimensionality through random projections [19]. Random projections provide a) an unified and coherent treatment of systematic and random errors; b) a compression tool, which can reduce the dimensionality of the data space; c) a noise model which is truly Gaussian therefore, making it therefore possible to apply rigorously Optimal Estimation Method (OEM) [20] and derive the correct retrieval uncertainty (often called error); d) a simplified treatment of the algebra to get the final solution, which greatly simplifies the computational burden of the inverse problem.

Another important aspect of this analysis was to check the HITRAN2012 compilation for OCS [21]. In fact, HITRAN2008 [22] was biased because of

a software error, e.g., see [21]. We have used HITRAN 2008 compilation for OCS in[13] and at the time we were not able to correctly recover the OCS seasonal cycle at Mauna Loa validation station. This was also the result of the fact that the retrieval configuration was not optimized for OCS. However, the final retrieval was significantly affected by OCS spectroscopic error. It is also important to stress that the software bug affected OCS alone [21]. All results shown in this study are based on HITRAN2012 OCS compilation [21], which does not contain this error.

OCS IASI retrievals are compared with in situ observations at the NOAA (National Oceanic and Atmospheric Administration) Mauna Loa laboratory, Hawaii, USA. We have also used one day of OCS measurements made by the same NOAA laboratory during the HIAPER (High-performance Instrument Airborne Platform for Environmental Research) Pole-to-Pole Observations (HIPPO) flights [23].

This paper is organized as follow. Section 2 summarizes data and methods. Section 3 will show the results and section 4 will be devoted to conclusions.

2. Data and methods

2.1. Data

The Infrared Atmospheric Sounder Interferometer or IASI [24] has been developed in France by CNES and is flying on board the Metop platforms. These are satellites of the EUMETSAT (European Organization for the Exploitation of Meteorological Satellite) European Polar System (EPS). IASI has been primarily designed as a meteorological mission, hence its main objective is to provide suitable information on temperature and water vapour profiles. The instrument has a spectral coverage extending from 645 to 2760 cm^{-1}, with a sampling interval $\Delta\sigma = 0.25$ cm^1 providing 8461 data points or channels for each single spectrum. Data samples are taken at intervals of 25 km along and across track, each sample having a minimum diameter (Field of View) of about 12 km. With

a swath width on Earths surface of about 2000 km, global coverage is achieved in 12 hours, during which the instrument records about 650000 spectra.

For the Hawaii region of interest to this study (see Fig. 1), a total of 43842 IASI spectra were acquired between Jan. 2014 to Dec. 2015. They are fully described in [13]. Moreover 6982 IASI soundings were acquired for the target area shown in Fig.2, which corresponds to the HIPPO flight overpass on August 29-30, 2011 (flight start: 29 August 2011, 22:23:33 UTC; flight end:30-Aug-2011 06:44:36). Further we use for this work IASI spectra measured above the Po Valley, Italy. A total of 137474 IASI soundings over this target area (see Fig. 3) have been analysed, which covers the whole year 2015. All IASI data have been screened for clear sky by considering the AVHRR (Advanced Very High Resolution Radiometer) native cloud mask. The data were then further screened by using the cloud mask algorithm developed in [25].

For the Hawaii region, representative OCS flask weekly data were collected at both stations of Mauna Loa (short name MLO, 19.5362 °N, 155.5763 °W, 3397 m asl) and Cape Kumukahi, (short name KUM, 19.516 °N, 154.811 °W, 3 m asl) for the period Jan. 2014 to Dec. 2015. MLO and KUM observatories in Hawaii are part of NOAA Earth System Research Laboratory (ESRL) and Global Monitoring Division (GMD). OCS data were downloaded from the website http://www.esrl.noaa.gov/gmd/hats/gases/OCS.html (see also [3] for a detailed description of these data). The surface data is reported in dry-air mole fraction i.e. pmol/mol for OCS and corresponding measurements from these sites and HIPPO flight results are traceable to NOAA calibration standards, whereas the IASI derived OCS column averaged dry air volume mixing ratio (VMR is the usual notation) are reported in ppmv. At the accuracy level of the remote sensing measurements we consider here that the in situ mole fractions in pmol/mol (or ppt) and remote sensed mixing ratios (in pptv) are equivalent. KUM is a station at sea level (3 m asl), whereas MLO is at an altitude of 3397 m asl and, therefore MLO data are likely more representative of OCS in the free troposphere (see also [3]), to which IASI is most sensitive. The comparison of MLO to KUM OCS (see Fig. 4) could be indicative of how much the

seasonal cycle amplitude is attenuated with altitude. An important result of this comparison is that the overall two-year mean OCS mole fraction at MLO (high altitude) is the same as that for KUM (sea level), that is 513.0 ppt at MLO and exactly the same value (up to the last digit) of 513.0 ppt at KUM during the 2014-2015 period. This good agreement also characterizes the yearly mean. For 2014 we have 514.3 (MLO) and 514.8 ppt (KUM); for 2015, 511.6 ppt (MLO) and 511.2 ppt (KUM). This shows that the OCS yearly mean is quite insensitive to altitude in the clean Hawaiian region, at least within the troposphere. Since OCS IASI retrievals are sensitive in the free troposphere, as we will show in section 2, their yearly mean should be consistent with that of in situ observations, despite of the fact that the in situ results represent point measurements and not column abundances. In this respect, it should be also stressed that additional NOAA observations (unpublished) suggest that there is no appreciable vertical gradient up to 8 km over the Hawaii MLO station at 3.4 km altitude, although there is a slight gradient ($\approx$ 1% higher mole fractions) below it.

As said, HIPPO data were acquired during a flight on 29-30 August 2011. Although HIPPO data sets cover a pole-to-pole latitudinal transect, the data used in the present study extend on a latitudinal belt some 30° wide (see Fig. 2). These data will be referred to as HIPPO5. The data were downloaded from the website `http://hippo.ucar.edu/`. Considering all the flask measurements made during the HIPPO flight we can form an OCS profile (see Fig. 5) which covers homogeneously the altitude range 0-15 km. The variability of these data is some 20% (see Fig. 5) in the altitude range 10-15 km and less than 10% in the lower troposphere, leading us to conclude that the profile presented in Fig. 4 is representative of the large target area of Fig. 2. For later comparison to IASI retrievals the original HIPPO5 data shown in Fig. 5 have been interpolated-extrapolated to the pressure-grid of our forward model (60 pressure layers from 1050 to 0.005 hPa). In the lower troposphere, the data have been simply continued down to the pressure surface using the HIPPO5 OCS value at the lowest altitude, whereas in the upper part of the atmosphere, they have been continued

by using the OCS AFGL (Air Force Geophysical Laboratory) reference profile [18]. The resulting profile is shown in Fig.6. Based on this profile, we estimated a column averaged VMR of 446.8 pptv, to be compared with the value of 510.8 pptv corresponding to the AFGL profile.

2.2. Retrieval Methodology

The retrieval methodology has been described in detail in [13]. Here, we outline only the main elements of the procedure, in which the full IASI spectrum (8461 channels) is used to simultaneously retrieve, the atmospheric profiles of temperature (T), water vapour (Q), ozone (O), and HDO, the surface temperature (T_s), and the columnar amount of CO_2, N_2O, CO, CH_4, SO_2, HNO_3, NH_3, OCS and CF_4. For land, the methodology retrieves also surface emissivity (ε). The emissivity spectrum (at IASI sampling of 0.25 cm^{-1}) is parameterized through a truncated Principal Component (PC) transform. The first 20 PC scores are retained, hence retrieved. For sea surface, emissivity is not retrieved and the Masuda model [26] is imposed to the retrieval.

An important improvement over the version used in[13] is the dimensionality reduction of the data space through random projections (RP) (e.g., [19]). RP is a linear transform that maps the original N dimensional data space (radiance vector in our analysis) into a n-dimensional ($n << N$) subspace, using a random $n \times N$ dimensional matrix $\mathbf{\Phi}$ whose rows are independent and identically distributed random variables from a Gaussian probability density function with a mean zero and a variance of $1/N$;

$$\mathbf{c} = \mathbf{\Phi R} \tag{1}$$

with $\mathbf{R}$ a generic radiance vector of size N and $\mathbf{c}$ is the vector of RP scores of size n. The vector $\mathbf{c}$ can be thought of as an incoherent sampling of the radiance vector. This incoherent sampling preserves the norm or vector length (see e.g. [19]) and allows us to reduce the dimensionality of IASI observations from 8461 channels to 1200 RP scores (see Tab. 1). In addition to the dimensionality reduction, the transform is providing a consistent and unified treatment of both

systematic and random error sources affecting the infrared observations. The property of the transform and its application to inverse problems have been discussed at a length in [19]. Here we limit ourselves to summarize those elements, which are specific to the present application.

Random projections can be applied to the full IASI spectral range, or segments of the spectral range. We use the latter strategy, because it allows us to better address the forward model noise, which depends on the wavenumber (see [19] for details). In our case, the IASI spectral coverage is broken in seven consecutive spectral intervals defined as shown in Tab. 1. Each single spectral interval is transformed with its own $\mathbf{\Phi}_j, j = 1, \ldots, 7$. Unlike the IASI original measurement errors, for each spectral interval, the random projected noise is independent of wavenumber and reduces to a single scalar term, given by [19]

$$s^2_{j,M+F} = \lambda^2_{j,F} s^2_{j,M}; \quad j = 1, \ldots, 7 \tag{2}$$

Here M stands for measurement error and F for forward model error. Moreover,

$$s^2_{j,M} = \frac{1}{N_j} \sum_{\sigma} s^2_j(\sigma); \quad j = 1, \ldots, 7 \tag{3}$$

where σ is the wavenumber, $s^2_j(\sigma)$ is the wavenumber-dependent IASI radiometric noise, the summation is over the wavenumber range, and N_j is the number of original spectral data points, defined for each spectral interval, j as shown in Tab.1. Finally, $\lambda^2_{j,F}$ is an inflation factor term, which takes into account the forward model bias. Within the random projection scheme, the forward bias is randomized, therefore we can consider both random component and forward model bias in a single variance term $s^2_{j,M+F}$. It is important to stress that noise correlations among wavenumbers are zeroed by the transform, and for each spectral interval, the noise is represented by a scalar variance in the form of $s^2_{j,M+F}$. Since for any pair, j_1, j_2 of the index j, the transforms $\mathbf{\Phi}_{j_1}$, $\mathbf{\Phi}_{j_2}$, are orthogonal, cross-correlation among spectral intervals are zeroed as well, therefore the observational covariance, once projected to the RP space, has a

block-diagonal structure, in which each block is a diagonal matrix itself,

$$\mathbf{S}_\epsilon = \begin{pmatrix} \lambda^2_{1,F} s^2_{1,M} \mathbf{I}_1 & \dots & \mathbf{0} \\ \dots & \dots & \dots \\ \mathbf{0} & \dots & \lambda^2_{7,F} s^2_{7,M} \mathbf{I}_7 \end{pmatrix} \tag{4}$$

where $\mathbf{I}_j, \quad j = 1, \dots 7$ is the diagonal matrix (size $n_j \times n_j$) pertinent to the j-th spectral interval.

The inflation factor, $\lambda^2_{j,F}$ could be fixed in many ways. The choice made here (see Tab.1) is based on trial and error, and is justified by an independent analysis of the forward model bias (see e.g., [13]). One important aspect of the methodology is that the total noise, $s^2_{j,M+F}$ can be estimated from variance of the spectral residual in the random projection space, i.e. $\hat{s}^2_{j,M+F}$. Then, we expect that the ratio, $Q_{j,I}$

$$Q_{j,I} = \frac{\lambda^2_{j,F} s^2_{j,M}}{\hat{s}^2_{j,M+F}} \geq 1; \quad \text{for each } j \tag{5}$$

Otherwise, the reverse would indicate that the prescribed noise, $\lambda^2_{j,F} s^2_{j,M}$ is less than the actual noise, hence that one is over-fitting the data. In our scheme, $Q_{j,I}$ is used as a further quality index, and only if all quality indexes (one for each spectral intervals shown in Tab. 1) meet the condition above, the retrieval is considered to be satisfactory. According to the Morozov discrepancy or residue criterion (e.g., see [19]), the condition $Q_{j,I} \geq 1$ is indeed implementing a smoothing or regularization for the inverse solution. To complete the analysis, the IASI radiometric noise (level 1C noise) that we use in the present analysis has been obtained according to [27] and is shown in Fig. 7. Moreover, Tab. 1 also shows another interesting use of the inflation factor. If we do not want a given spectral interval to contribute to the final solution we can just prescribe for the spectral interval a very large $\lambda^2_{j,F}$. This is the case for the spectral interval 2240 to 2500 cm^{-1} in daytime because of non-LTE effects, which are not considered in our forward model. For the rest, we note that the smaller $\lambda^2_{j,F}$ is prescribed for the atmospheric window (800 to 1210 cm^{-1}) where the spectroscopy of contributing species is best known. For the water vapour band

at 6.7 μm a relatively larger inflation has to be applied because uncertainties in the water vapour spectroscopy (line shapes and their temperature dependence) and in the associated continuum absorption.

The inversion algorithm is based on the combination of a fully analytical, monochromatic radiative transfer model, and an OEM module [20]. The radiative transfer model is called σ-IASI [28, 29], and is a fast model, which uses a pre-computed look-up table for the optical depth calculation. The look-up table is derived from LBLRTM (Line-by-Line Radiative Transfer Model, [30], using the line compilation aer 3.2 (see e.g. `http://rtweb.aer.com/line_param_frame.html`), which adopts HITRAN 2008 [22], except for OCS for which the look-up table is based on the line compilation aer 3.4, which adopts HITRAN2012 [21]. As described in [21], HITRAN2008 OCS line parameters are not correct because of a bug in the HITRAN software.

We stress that the software bug affects the original HITRAN2008 OCS line compilation and not the way it is integrated in the aer 3.2 database. Therefore, OCS retrieval analysis based on HITRAN 2008 are likely in error. In fact, the bug can produce very different OCS optical depths as shown, e.g. in Fig. 8. In an early attempt to retrieve OCS from IASI we used HITRAN2008, which resulted in a large retrieval bias. The same significant bias is likely to affect the results shown in [11].

The forward module computes the radiance after discretizing the radiative transfer equation on a fixed grid made up by $N_L = 60$ pressure layers, which spans the atmosphere from 1050 to 0.005 hPa. The forward model yields spectral radiances and analytical Jacobians with respect to surface temperature, emissivity and any atmospheric parameter, including the VMR profile of H_2O, O_3, HDO, CO_2, N_2O, CO, CH_4, SO_2, HNO_3, NH_3, OCS and CF_4. In its latest version [29], σ-IASI also consider the sun spectral radiation, which may add an important contribution in the spectral interval 2000 to 2240 cm^{-1}, which contains most of the information for retrieving OCS. Forward model IASI radiances are obtained through convolution with the nominal IASI Instrumental Spectral Response Function (ISRF) at level L1C.

The inversion scheme, called δ-IASI [31] implements an iterative algorithm for the optimal estimation of the thermodynamic state of the atmosphere and its composition. The present version of δ-IASI has been modified according to [19] and include now a full treatment of the radiance space with random projections. The model δ-IASI performs the mathematical inversion of the whole IASI radiance spectrum (8461 channels) to simultaneously retrieve the state vector, which includes ε, T_s, T, Q, O and the minor and trace gases HDO, CO_2, N_2O, CO, CH_4, SO_2, HNO_3, NH_3, OCS, CF_4). One important aspect on the retrieval scheme, which is relevant to the estimation of trace gases, is the use of background (i.e. a priori, here and afterwards background and a priori are used as synonyms) and first guess state vectors, which are as much as possible in the linear region of the radiative transfer equation. Towards this objective we use ECMWF (European Centre for Medium range Weather Forecasts) analysis for (T, Q, O) collocated in space and time with the IASI soundings (see [13] for details). The use of ECMWF (T, Q, O) analysis is providing a strong constraint in the inverse scheme and we think that the corresponding profiles are reliable. This is allowing us to relax the constraints for the trace gases. In effect, their profiles are normally adjusted starting from a climatology as a first guess and the retrieved profiles reach their final values in one-two iterations. Therefore, in the case of OCS, the background profile for the corresponding part of the state vector is set equal to the reference profile (see Fig. 6).

2.2.1. OCS retrieval details

In our scheme, the column amount of a given trace gas can be retrieved either using a parametric method or a non-parametric approach. Both strategies require the computation of the OCS Jacobian derivatives at the full forward model spectral and vertical spatial resolution. The use of a single scaling factor to parameterize the OCS and other trace gas VMR profiles has been described at length in [13], which the reader is referred to for further details. Using the parametric method, a fixed profile shape (that of the background profile shown in Fig. 6) with a column averaged VMR of 510.8 pptv is used and we find

the scaling factor, f which gives a best match to the spectral observations. The background state for f is $f = 0$ (i.e., the column amount of the background profile) and its background variance is chosen equal to 4. This relatively large value ensures a good independence of the background with a value for the degrees of freedom (d.o.f.) equal to 1.

According to [20], the parametric or f-scaling approach is not generating the best estimate (in a Bayesian sense) of the column amount, and the a posteriori retrieval error could be underestimated. An alternative method, which according to [20] is optimal and yields the correct a posteriori error estimate is the non-parametric estimation approach, where a vector-valued profile $\mathbf{G}_{OCS}$ of size N_L (i.e., the number of layers in our forward model) is first retrieved and then the column amount, $\bar{G}_{OCS}$ is obtained according to

$$\bar{G}_{OCS} = \mathbf{h}^t \hat{\mathbf{G}}_{OCS}; \quad \text{var}(\bar{G}_{OCS}) = \mathbf{h}^t \mathbf{S}_{\hat{G}} \mathbf{h} \tag{6}$$

Here $\mathbf{S}_{\hat{G}}$ is the covariance matrix of the retrieved profile $\hat{\mathbf{G}}_{OCS}$, $\mathbf{h}$ the averaging operator (e.g. see [13]) and var$(\cdot)$ stands for variance. The column amount $\bar{G}_{OCS}$ is corrected for the effect of moist air as shown in [13].

The non-parametric approach needs a proper background state $\mathbf{G}_{OCS,a}$ and its covariance matrix $\mathbf{S}_{G_{OCS,a}}$. Once again, the retrieval independence of the background is reached provided the variance values $S_{G_{OCS,a}}(i,i) \to \infty; \quad i = 1, \ldots, N_L$, in which case we might extract all the N_L degrees of freedom available for the profile. However, this would happen to the expense of precision (in the sense of uncertainty or error bar), which tends to infinity. This is because the related unconstrained Least Squares problem to derive $\hat{\mathbf{G}}_{OCS}$ becomes singular and does not have a finite solution. Thus, a compromise between uncertainty and retrieval information content has to be found.

Coming back to the present analysis, the OCS background state vector, $\mathbf{G}_{OCS,a}$ is the reference profile shown in Fig. 6. For the background covariance, we consider the Markov-type matrix (e.g. [32]),

$$S_{G_{OCS,a}}(i,j) = \left(s_{OCS,a} G_{OCS,a}(i)\right) \left(s_{OCS,a} G_{OCS,a}(j)\right) \exp\left(\frac{-|i-j|}{l}\right) \tag{7}$$

In this equation, l is an appropriate length scale and the standard deviation of the profile at a given layer i is a fraction $s_{OCS,a}$ of the layer mixing ratio $G_{OCS,a}(i)$. Thus, the diagonal elements can get any value depending on $s_{OCS,a}$. The dependence of both dof and precision on $s_{OCS,a}$ can be obtained in simulation, based on a linear error analysis. To exemplify the expected performance, we have used a tropical air mass (ECMWF analysis for the Hawaii region) with $s_{OCS,a} = 2, l = 1$ in Eq. 7. With $s_{OCS,a} = 2$, we let the profile vary by about 200% around the background at each layer. Furthermore, with $l = 1$, the background covariance matrix is nearly diagonal.

Moving l from zero to infinity we can trade-off between spatial vertical resolution and accuracy. The approach we have taken in this paper is to privilege spatial vertical resolution and compensate for the loss of accuracy through averaging over many OCS retrievals. Our objective is to be as much as possible independent of the a priori profile. We aim at showing that the retrieval of reliable OCS atmospheric load can be obtained also for regions where good *a-priori* information is not available, a fact which is relevant to OCS and other gas species. However, we stress that this choice is specific to our objective and has not to be meant as a general rule. In effect, there are cases, e.g. CO_2, which could benefit from a larger l. Furthermore, we stress again that we are not interested in the OCS profile retrieved from a single, individual IASI observation, which with the adopted loose constraint ($s_{OCS,a} = 2, l = 1$) is meaningful because of large oscillations. We are primarily interested in getting an estimate of the total load and those oscillations are offset when we integrate over the atmospheric column.

Figure 9 shows the Averaging Kernels (AK) for the retrieved OCS profile. As expected, AK peaks below 0.2, which means that the retrieval will be largely dependent on the background. In fact, the degrees of freedom (d.o.f.), computed as the trace of AK, are d.o.f.≈ 1. However, once again we stress that our goal is to obtain a valuable estimate for the column amount.

For the column amount, the background error is some 40% to be compared with the expected retrieval error (square root of the a posteriori variance, see

Eq. 6) of $\approx 20\%$. An expected retrieval performance of 20% for the single IASI observations is satisfactory considering that the typical time scale of OCS is several days, so that many IASI daily observations can be averaged to improve precision.

If $\mathbf{A}$ is the averaging kernels matrix for OCS, that for the column amount is $\mathbf{h}^t\mathbf{A}$ and is plotted in Fig. 10. However, the meaning of this last quantity is conceptually different from that of the usual averaging kernels, $\mathbf{A}$ [33], since $\bar{G}_{OCS}$ is not part of the state vector. Figure 10 is just aiming at comparing $\mathbf{h}^t\mathbf{A}$ to $\mathbf{h}^t$. In fact, in a perfect retrieval $\mathbf{A}$ would be the identity matrix and we should have $\mathbf{h}^t\mathbf{A} = \mathbf{h}^t$. It is interesting to see that the weights $\mathbf{h}^t\mathbf{A}$ remains positive and different from zero throughout the atmosphere. They are smaller in the lower troposphere because, for each pressure layer j, they are proportional to $\frac{p_j - p_{j+1}}{p_o}$; $\quad j = 1, \ldots, N_L$ with p_o the pressure of the lowermost layer. This effect is also seen for the original weights,$\mathbf{h}^t$. They are smaller in the lower troposphere because of the denser layering in that part of the atmosphere. We also stress that for our objective of estimating the column amount, the broad structure of AK rows (see Fig. 9) shows that information is spread throughout the vertical altitude and can be gained under profile integration, hence the good sensitivity to the column amount as shown in Fig. 10.

As far as smoothing constraints are concerned, they could increase by applying a stronger smoothing constraint to the OCS retrieval, e.g., by increasing the length scale, l and/or using a smaller value for the standard deviation, $s_{OCS,a}$ in Eq. 7 (6). However, both larger, l and smaller, $s_{OCS,a}$ would increase the dependence of OCS retrieval on the background. One should consider that even with the very loose constraint we use, d.o.f.$\approx$ 1, which would inevitably get smaller by using larger smoothing.

To sum up, when using the scaling approach for OCS we retrieve the state vector, (T_s,$\mathbf{T}$,$\mathbf{Q}$,$\mathbf{O}$,$\mathbf{HDO}$,f_{CO_2},f_{N_2O},f_{CO},f_{CH_4},f_{SO_2},f_{HNO_3},f_{NH_3},f_{OCS},f_{CF_4}) , where bold quantities mean that we retrieve the profile and f_X means scaling factor for the given species X. With the non-parametric approach for OCS the state vector is (T_s,$\mathbf{T}$,$\mathbf{Q}$,$\mathbf{O}$,$\mathbf{HDO}$,$\mathbf{OCS}$,f_{CO_2},f_{N_2O},f_{CO},f_{CH_4},f_{SO_2},f_{HNO_3},f_{NH_3},f_{CF_4}).

In the two approaches, the observational covariance matrix, $\mathbf{S}_\epsilon$ is simplified because the forward model parameter error source is zeroed and $\mathbf{S}_\epsilon$ is made dependent on the IASI measurement noise and forward model bias alone. In effect, the time to complete the run for one single IASI spectrum is that of the forward model, which involves the computation of the IASI spectrum and 14 Jacobian matrix derivatives at each iteration.

It is worth noting that thanks to the use of random projections, the computational burden of the retrieval scheme has been reduced a lot in comparison with the version used previously. The typical time of a single run is ≈ 7 s considering a platform with an IntelCore i7-2600CPU3.50 GHz. This time can be optimized because at present our software is based on a hybrid Matlab-Fortran architecture. Since IASI reaches the global coverage in 12 hours, during which the instrument records about 650000 spectra, of which some 20% in clear sky, with a commercial work station equipped with some 50-100 CPUs, our inverse scheme can easily run in real time even in its present non-optimized software architecture.

Finally, we stress that for the results presented in the next section both retrieval approaches are using random projections (the data space is reduced exactly the same way) as well as the HITRAN2012 compilation for OCS. HITRAN2008 for OCS has been definitely dismissed because of the software bugs [21] discussed in section 2.2 (see also Fig. 8).

3. Results

First, we will discuss the results for the two case studies of HIPPO5 flight and MLO station, then an application to land surface (where seasonal and spatial variability is higher) will be described. To begin with, we start with the HIPPO5 case study.

3.1. HIPPO5 flight

For this case study, we have a total of 6982 IASI, daytime, soundings, of which 656 were in clear sky. After running the retrieval scheme, 415 soundings

were successfully inverted with proper consideration of the quality check condition of Eq. 5. For the non-parametric approach, the retrieved OCS profiles are shown in Fig. 11 along with the background VMR profile. We see that the retrievals cover a range of VMR values, although the average profile shape is quite consistent with the background shape. However, there is a tendency to retrieve smaller OCS amounts than the background value. Averaging all retrievals, we have obtained the mean OCS profile shown in Fig. 12, which is compared to the original HIPPO5 profile (denoted with $\mathbf{G}_{H5}$) and the HIPPO5_AK profile (denoted with $\mathbf{G}_{H5AK}$), which is projected in the IASI retrieval space through the linear relation,

$$\mathbf{G}_{H5AK} = \mathbf{G}_{OCS,a} + \mathbf{A}\,(\mathbf{G}_{H5} - \mathbf{G}_{OCS,a}) \tag{8}$$

In this equation $\mathbf{A}$ is the averaging kernels matrix obtained by averaging the 415 retrievals. Each sounding can be considered as independent from the other ones since the characteristics of any given sounding (IASI pixel number, position along the swath, time and location) are largely uncorrelated. Hence the statistical reduction of the uncertainty on the mean by the square root of the number of measurements is justified. It is seen that HIPPO5_AK is smoother and similar to the mean retrieved profile. However, differences between the retrieval and HIPPO5 are seen, which can be understood considering that HIPPO5 is not an exact vertical profile (because of some possible horizontal gradient) and that the retrieval has barely a d.o.f.= 1. Much more interesting for us is the comparison for the column averaged VMR. The retrieval mean is (447.9 ± 2.6) pptv, where the error has been computed considering the standard deviation of the 415 retrievals divided by the square root of 415. The above estimate can be compared with the derived HIPPO5 column averaged VMR of 446.8 pptv. To sum up, the non-parametric approach yields a result which is largely unbiased and correctly moves away from the background of 510 pptv.

For the scaling approach the convergence was achieved for 435 soundings (20 more than the non-parametric approach). The retrieval mean is (378.5 ± 5.0) pptv, which is largely biased with respect to HIPPO5. Also it is interesting to

note that with the parametric approach the variability of the retrieval is almost doubled.

For a proper comparison between parametric and non-parametric approach, it should be stressed that in both cases the final aim is to estimate OCS column amount. In other words, the non-parametric approach is not intended for OCS profile estimation. In fact, there is only about 1 degree of freedom available. The degree of freedom is not localized (e.g. AK peak equal to 1 at given layer and zero otherwise) and we cannot say if the profile is behaving better at some level altitude. The 1 degree of freedom is gained when we perform profile integration over the vertical to get the average column amount. Thus, parametric and non-parametric approach should be compared in their ability to derive the OCS column amount. Finally, we also stress that according to [20], the best estimate (in a Bayesian sense) of the column amount is achieved with the non-parametric approach.

One could also pose the question why the parametric approach is significantly biased. The bias structure of the f-approach depends on the background or a priori profile, which can simply be scaled but not adjusted vertically. Figure 12 exemplifies how in this case the shape of the background is different from that of in situ measurements, which are supposed to be closer to truth. This difference is enhancing the bias in the retrieval. In contrast, the non-parametric approach can adjust the profile in the vertical dimension. Given d.o.f. ≈ 1, the added freedom has a poor effect on the profile itself, but becomes important for the estimation of the integrated column amount. Finally, it should be stressed that a proper choice of the *a priori* profile could improve the performance of the f-approach and yield lower bias.

3.2. Seasonal variations and comparison with MLO data

For the Hawaii case study, we have exploited two years (Jan. 2014 to Dec. 2015) of IASI soundings for the target area shown in Fig. 1. As said in section 2, MLO and KUM data are point measurements therefore we do not expect a perfect match with IASI retrievals, which are sensitive to the atmospheric

column. However, the comparison is important to check if IASI is sensitive to seasonal variations.

As for the HIPPO5 case study, we have performed the retrieval exercise for both the parametric (scaling) and non-parametric approach. Comparison of OCS retrieved and in situ observations will be shown mostly for MLO, since this station is more representative than KUM of OCS in the free troposphere, to which IASI is sensitive. We begin with the non-parametric approach.

Figure 13 exemplifies the IASI retrieved monthly profile for Jan. 2014 and May 2014. According to the surface data in Fig.4, OCS attains its peak value in May and we see that the monthly column corresponding to May (see Fig. 14) shows a larger OCS density than that for January. In effect, IASI is sensitive to seasonal variations as it is possible to see from Fig. 14, which shows the monthly means from Jan. 2014 to Dec. 2015. Although the individual MLO monthly mean values sample only a limited portion (in space and time) of the variability of the OCS column, we expect that on average (two years), the mean at MLO and that of IASI retrievals have to be largely consistent. In fact, as shown in section 2 (see Fig. 4 and [3]), the mean is fairly independent with altitude. For the case of night-time IASI soundings (see Fig. 10 for the column retrieval sensitivity), we extract a mean tropospheric mixing ratio of (514.1 ± 1.0) pptv to be compared with a mole fraction of 513.0 ppt at MLO and (the same value) of 513.0 ppt at KUM. There is a difference between IASI retrieval and in situ observations of about 1 pptv. It is important to stress that the retrieval of the column averaged OCS mixing ratio shown in Fig. 14 is based on a background profile fixed in time (see the a priori or background in Fig. 6), therefore the IASI capability of detecting the cycle is genuine information from data alone.

For a remote high-altitude station, such as MLO, we do not expect OCS to show day-night variations, since the main source of OCS is the ocean. This means that day time IASI retrievals have to be consistent with those at night time. Day time retrievals are possibly made difficult because of sun radiation, which adds a non-negligible contribution for wavenumbers higher than 2000 cm^{-1}. By performing daytime retrievals, we can also check the quality of the

sun module of our forward model [29].

Figure 14 also shows day time soundings. It is seen that the OCS cycle is fairly well reproduced. Furthermore, we estimate a mean (over the 2 year period) of (511.8 ± 1.1) pptv, which again is consistent with the KUM and MLO observations.

The consistency of night and day time soundings is further evidenced when we consider their combination, agian shown in Fig. 14. Considering both day and night time IASI soundings improves the correlation to 0.89 with MLO observations (collected during the morning) and reduces the difference in the mean to nearly zero. Another important aspect of the analysis is that IASI retrieval can resolve almost the full amplitude of the seasonal cycle. This is an interesting results also in view of possible assimilation of IASI OCS retrieval in models of global cycles of OCS and CO_2 [9]. According to [9], present models fail to correctly represent the OCS cycle at Mauna Loa station.

As far as the accuracy of the scaling or parametric approach, Fig. 14 summarizes the results for day time IASI soundings (for night we obtained equivalent results, which are not shown for the sake of brevity). We see that the amplitude and phase of the OCS cycle are correctly reproduced with both approaches. However, the scaling approach lacks consistency in the two year mean. We observe a difference with in situ observations of some 22-25 pptv for both day and night soundings. This difference is less pronounced than that seen for the HIPPO5 case study, but it is real, nevertheless, and the scaling approach is producing values that are less consistent when compared to the mean abundance observed with in situ surface observations (as expected if small vertical gradients are present). The scaling approach seems to be capable of extracting the correct cycle and spatial gradients, but it has a bias whose structure can depend on time and space. As also discussed at the end of section 3.1 when dealing with the f-scaling approach, this is an indication that a single f-background profile is not appropriate for all time and location. In effect, the f-scaling method coud be improved by choosing an appropriate *a priori* .

3.3. Application to land surface (preliminary results)

This retrieval example is mainly intended to demonstrate the capability of the method to run also above land surface, in which case we have to consistently retrieve surface emissivity. The analysis applies to the Po Valley in Italy, which is characterized by intense farming and other intense activity linked to agriculture. The rationale of the analysis is to demonstrate that IASI is sensitive to the OCS seasonal cycle over a region, which is characterized by leaf and soil sources/sinks.

For this case study, we limit ourselves to the non-parametric approach. The retrieved state vector is ($\varepsilon(\sigma)$, T_s, **T**, **Q**,**O**, **HDO**, **OCS**, f_{CO_2}, f_{N_2O}, f_{CO}, f_{CH_4}, f_{SO_2}, f_{HNO_3}, f_{NH_3}, f_{CF_4}) where $\varepsilon(\sigma)$) is the surface emissivity spectrum over the IASI spectral coverage, 645 to 2760 cm^{-1}.

Figures 15 and 16 summarize the OCS monthly mean for February and August, respectively. The year is 2015. To help in recognizing spatial patterns the maps shown in these two figures are contour maps. Furthermore, to help to geo-locate patterns, the map is super-imposed to a Google^{TM}Earth view of the target area.

For both maps, forest canopies tend to correspond to higher OCS column amount. Forest canopies extend along the North-South-West borders of the maps, following the structure of the Alps-Apennines chains. The Δ-shaped Po Valley opens to the East, toward the Adriatic Sea. As said, this is the region is mostly involving intense farming.

February and August are close to the OCS cycle maximum and minimum, respectively. The timing of uptake from soils and/or plants has been discussed in [3]. Figures 15 and 16 show that patches with a relative smaller OCS column amounts tend to form in the valley, an effect which may hint at a spatial variability in OCS uptake in the forest canopy compared to agricultural soil region. This difference could also be intensified here because of orography and the peculiar meteorological characteristics of the Po Valley: weather regimes of relatively poor turbulent mixing of the boundary layer, with conditions of wet and stagnant air, which can last for weeks. In effect, the Po Valley is unique because the pollutants are trapped in the valley, and therefore, the pollutant

signals are stronger than in more ventilated open areas (e.g. [34]).This means that the canopy and agricultural field ecosystems marked in Fig. 3 are geographically and meteorologically separated. A possible difference of OCS intake from canopy and soil should be evidenced by an analysis of monthly OCS time series. The analysis of the IASI OCS column averaged mixing ratio (mostly tropospheric) is provided in Fig. 17. Not only are the agricultural fields more effective at removing OCS from the atmosphere, the cycle itself has a slightly different behaviour. For the forest canopy the minimum is reached in June when we have the longest sunshine duration. In the Po Valley, the agricultural fields seem to be more effective in removing OCS in August. In effect, according to [7] the process of soil OCS uptake is enhanced with increasing temperature (an optimal soil temperature is around 25 °C) and lower soil moisture, which are more likely in August.

For the proper understanding of the results shown in this section, we remark that we consider only OCS retrievals corresponding to a thermodynamic structure of the troposphere with no thermal inversion in the boundary layer, that is we consider retrievals corresponding to a negative lapse rate alone. In effect, these are conditions, which favour a vertical expansion of the boundary layer. The temperature lapse-rate screening can be done easily in our scheme, because temperature and humidity are simultaneously retrieved with gases. This screening should avoid artefacts due to changing thermal contrast of land-atmosphere. In particular, positive lapse rate (temperature inversion in the boundary layer) tends to give negative AK in the lower troposphere, which artificially depletes the column amount. This effect is minimized in our retrievals.

Finally, it should be stressed that, according to [7, 10], consumption by soils dominates OCS emission from soils and its contribution to the global atmospheric budget is large, at about one third of the OCS uptake by vegetation (see also [1]). The effect of soil uptake is irreversible and may also be measurable at a local scale. Nevertheless, we stress that the application shown in this section is demonstrative and that our results are preliminary. Further work is needed before deriving firm conclusions.

4. Conclusions

An assessment of the IASI capability for yielding estimate of OCS column amount has been presented in this paper. We have shown that IASI is sensitive to the OCS seasonal cycle over ocean. Seasonal cycle amplitude, phase and mean level can be retrieved with high accuracy and precision, provided we use the HITRAN 2012 compilation. HITRAN 2008 compilation for OCS is affected by serious errors and should not be used. Heavy biases found in early works (e.g., [11]) are likely the effect of wrong OCS spectroscopy.

The analysis has also provided a comparison between two retrieval approaches: the scaling or parametric approach in which a known OCS profile is parameterized with a single scaling factor, and the non-parametric approach, which takes into account the full dependence of the radiative transfer equation on the exact OCS profile. In this approach, the OCS profile is retrieved on the 60-layers pressure grid of the forward model and the column abundance is computed by a proper averaging integration (operator $\mathbf{h}^t$) over the profile. This second approach is by far better in terms of bias and precision error. The parametric approach is significantly biased although it seems to correctly extract seasonal cycle amplitude and phase.

Finally, we have exemplified the methodology for land surface with the aim of checking the sensitivity of IASI to the seasonal cycle for ecosystems dominated by soil and/or leaf in a region with intense agricultural and farming activities. We have shown that IASI captures the seasonal cycle expected for these ecosystems. However, this part of the study is mainly demonstrative and further analysis, which we will be performed near future, is needed before deriving firm conclusions.

5. Acknowledgements

In situ observations recorded at Mauna Loa and Cape Kumukahi Observatories in Hawaii have been downloaded from the web site `http://www.esrl.noaa.gov/gmd/hats/gases/OCS.html`. HIPPO 5 data have been downloaded

from the web page `http://hippo.ucar.edu/`. We give credit to the National Oceanic and Atmospheric Administration (NOAA)/Global Monitoring Division (GMD) in Boulder as a source of the data and the work of F. Moore, E. Atlas, S. Wofsy and others for making the HIPPO measurements possible. IASI has been developed and built under the responsibility of the Centre National dEtudes Spatiales (CNES, France). It is flown on board the Metop satellites as part of the EUMETSAT Polar System. The IASI L1C data are received through the EUMETCast near real time data distribution service. The background Po Valley maps of Figures 3, 15 and 16 have been reproduced from Google^{TM} Earth. This research was carried out in the framework of the project *Smart Basilicata* which was approved by the Italian Ministry of Education, University and Research (MIUR D.M. n.2078/2015) and was funded with the Cohesion Fund 20072013 of the Basilicata Regional authority (Grant n. 6386-3/2016). We would like to thank two anonymous reviewers for valuable comments and remarks, which improved the paper.

References

References

[1] D. Asaf, E. Rotenberg, F. Tatarinov, U. Dicken, S. Montzka, D. Yakir, Ecosystem photosynthesis inferred from measurements of carbonyl sulphide flux, Nature Geosci. 6 (2013) 186–190.

[2] K. Maysek, J. Berry, D. Billesbach, J. Campbell, M. Torn, M. Zahniser, U. Seibt, Sources and sinks of carbonyl sulfide in an agricultural field in the southern great plains, Proceedings of the National Academy of Sciences 111 (25) (2013) 9064–9069.

[3] S. A. Montzka, P. Calvert, B. D. Hall, J. W. Elkins, T. J. Conway, P. P. Tans, C. Sweeney, On the global distribution, seasonality, and budget of atmospheric carbonyl sulfide (cos) and some similarities to co2, Journal of Geophysical Research: Atmospheres 112 (D9) (2007) n/a–n/a, d09302.

doi:10.1029/2006JD007665.
URL http://dx.doi.org/10.1029/2006JD007665

[4] M. Ko, et al., Very short-lived halogen and sulfur substances, in scientific assessment of ozone depletion, Global Ozone Res. Monit. Proj., WMO, Geneva.

[5] M. Chin, D. D. Davis, Global sources and sinks of ocs and cs2 and their distributions, Global Biogeochemical Cycles 7 (2) (1993) 321–337. doi:10.1029/93GB00568.
URL http://dx.doi.org/10.1029/93GB00568

[6] J. E. Campbell, G. R. Carmichael, T. Chai, M. Mena-Carrasco, Y. Tang, D. R. Blake, N. J. Blake, S. A. Vay, G. J. Collatz, I. Baker, J. A. Berry, S. A. Montzka, C. Sweeney, J. L. Schnoor, C. O. Stanier, Photosynthetic control of atmospheric carbonyl sulfide during the growing season 322 (5904) (2008) 1085–1088. doi:10.1126/science.1164015.

[7] J. Ogée, J. Sauze, J. Kesselmeier, B. Genty, H. Van Diest, T. Launois, L. Wingate, A new mechanistic framework to predict ocs fluxes from soils, Biogeosciences 13 (8) (2016) 2221–2240. doi:10.5194/bg-13-2221-2016.
URL http://www.biogeosciences.net/13/2221/2016/

[8] J. E. Campbell, M. E. Whelan, U. Seibt, S. J. Smith, J. A. Berry, T. W. Hilton, Atmospheric carbonyl sulfide sources from anthropogenic activity: Implications for carbon cycle constraints, Geophysical Research Letters 42 (8) (2015) 3004–3010, 2015GL063445. doi:10.1002/2015GL063445.
URL http://dx.doi.org/10.1002/2015GL063445

[9] J. Berry, A. Wolf, J. E. Campbell, I. Baker, N. Blake, D. Blake, A. S. Denning, S. R. Kawa, S. A. Montzka, U. Seibt, K. Stimler, D. Yakir, Z. Zhu, A coupled model of the global cycles of carbonyl sulfide and co2: A possible new window on the carbon cycle, Journal of Geophysical Research: Biogeosciences 118 (2) (2013) 842–852. doi:10.1002/jgrg.20068.
URL http://dx.doi.org/10.1002/jgrg.20068

[10] T. Launois, P. Peylin, S. Belviso, B. Poulter, A new model of the global biogeochemical cycle of carbonyl sulfide part 2: Use of carbonyl sulfide to constrain gross primary productivity in current vegetation models, Atmospheric Chemistry and Physics 15 (16) (2015) 9285–9312. doi:10.5194/acp-15-9285-2015.
URL http://www.atmos-chem-phys.net/15/9285/2015/

[11] L. Kuai, J. Worden, S. S. Kulawik, S. A. Montzka, J. Liu, Characterization of aura tes carbonyl sulfide retrievals over ocean, Atmospheric Measurement Techniques 7 (1) (2014) 163–172. doi:10.5194/amt-7-163-2014.
URL http://www.atmos-meas-tech.net/7/163/2014/

[12] L. Kuai, J. R. Worden, J. E. Campbell, S. S. Kulawik, K.-F. Li, M. Lee, R. J. Weidner, S. A. Montzka, F. L. Moore, J. A. Berry, I. Baker, A. S. Denning, H. Bian, K. W. Bowman, J. Liu, Y. L. Yung, Estimate of carbonyl sulfide tropical oceanic surface fluxes using aura tropospheric emission spectrometer observations, Journal of Geophysical Research: Atmospheres 120 (20) (2015) 11,012–11,023, 2015JD023493. doi:10.1002/2015JD023493.
URL http://dx.doi.org/10.1002/2015JD023493

[13] G. Liuzzi, G. Masiello, C. Serio, S. Venafra, C. Camy-Peyret, Physical inversion of the full {IASI} spectra: Assessment of atmospheric parameters retrievals, consistency of spectroscopy and forward modelling, Journal of Quantitative Spectroscopy and Radiative Transfer 182 (2016) 128 – 157. doi:https://doi.org/10.1016/j.jqsrt.2016.05.022.
URL http://www.sciencedirect.com/science/article/pii/S0022407316301248

[14] R. A. Vincent, A. Dudhia, Fast retrievals of tropospheric carbonyl sulfide with iasi, Atmospheric Chemistry and Physics 17 (4) (2017) 2981–3000. doi:10.5194/acp-17-2981-2017.
URL http://www.atmos-chem-phys.net/17/2981/2017/

[15] K. A. Tereszchuk, G. González Abad, C. Clerbaux, J. Hadji-Lazaro, D. Hurtmans, P.-F. Coheur, P. F. Bernath, Ace-fts observations of pyrogenic trace species in boreal biomass burning plumes during bortas, Atmospheric Chemistry and Physics 13 (9) (2013) 4529–4541. doi:10.5194/acp-13-4529-2013.
URL http://www.atmos-chem-phys.net/13/4529/2013/

[16] N. Glatthor, M. Höpfner, A. Leyser, G. P. Stiller, T. von Clarmann, U. Grabowski, S. Kellmann, A. Linden, B.-M. Sinnhuber, G. Krysztofiak, K. A. Walker, Global carbonyl sulfide (ocs) measured by mipas/envisat during 2002–2012, Atmospheric Chemistry and Physics 17 (4) (2017) 2631–2652. doi:10.5194/acp-17-2631-2017.
URL http://www.atmos-chem-phys.net/17/2631/2017/

[17] J. E. Johnson, The lifetime of carbonyl sulfide in the troposphere, Geophysical Research Letters 8 (8) (1981) 938–940. doi:10.1029/GL008i008p00938.
URL http://dx.doi.org/10.1029/GL008i008p00938

[18] G. P. Anderson, S. A. Clough, F. X. Kneizys, J. H. Chetwynd, E. P. Shettle, AFGL atmospheric constituent profiles (0–120 km).

[19] C. Serio, G. Masiello, G. Liuzzi, Demonstration of random projections applied to the retrieval problem of geophysical parameters from hyperspectral infrared observations, Appl. Opt. 55 (24) (2016) 6576–6587. doi:10.1364/AO.55.006576.
URL http://ao.osa.org/abstract.cfm?URI=ao-55-24-6576

[20] C. D. Rodgers, Inverse methods for atmopsheric sounding: Theory and practice, World Scientific, Singapore, 2000.

[21] L. Rothman, I. Gordon, Y. Babikov, A. Barbe, D. C. Benner, P. Bernath, M. Birk, L. Bizzocchi, V. Boudon, L. Brown, A. Campargue, K. Chance, E. Cohen, L. Coudert, V. Devi, B. Drouin, A. Fayt, J.-M. Flaud,

R. Gamache, J. Harrison, J.-M. Hartmann, C. Hill, J. Hodges, D. Jacquemart, A. Jolly, J. Lamouroux, R. L. Roy, G. Li, D. Long, O. Lyulin, C. Mackie, S. Massie, S. Mikhailenko, H. Mller, O. Naumenko, A. Nikitin, J. Orphal, V. Perevalov, A. Perrin, E. Polovtseva, C. Richard, M. Smith, E. Starikova, K. Sung, S. Tashkun, J. Tennyson, G. Toon, V. Tyuterev, G. Wagner, The {HITRAN2012} molecular spectroscopic database, Journal of Quantitative Spectroscopy and Radiative Transfer 130 (2013) 4 – 50, {HITRAN2012} special issue. doi:https://doi.org/10.1016/j.jqsrt.2013.07.002.
URL http://www.sciencedirect.com/science/article/pii/S0022407313002859

[22] L. Rothman, I. Gordon, A. Barbe, D. Benner, P. Bernath, M. Birk, V. Boudon, L. Brown, A. Campargue, J.-P. Champion, K. Chance, L. Coudert, V. Dana, V. Devi, S. Fally, J.-M. Flaud, R. Gamache, A. Goldman, D. Jacquemart, I. Kleiner, N. Lacome, W. Lafferty, J.-Y. Mandin, S. Massie, S. Mikhailenko, C. Miller, N. Moazzen-Ahmadi, O. Naumenko, A. Nikitin, J. Orphal, V. Perevalov, A. Perrin, A. Predoi-Cross, C. Rinsland, M. Rotger, M. imekov, M. Smith, K. Sung, S. Tashkun, J. Tennyson, R. Toth, A. Vandaele, J. V. Auwera, The {HITRAN} 2008 molecular spectroscopic database, Journal of Quantitative Spectroscopy and Radiative Transfer 110 (910) (2009) 533 – 572, {HITRAN}. doi:https://doi.org/10.1016/j.jqsrt.2009.02.013.
URL http://www.sciencedirect.com/science/article/pii/S0022407309000727

[23] S. C. Wofsy, the hippo science team and cooperating modellers and satellite teams, hiaper pole-to-pole observations (hippo): fine-grained, global-scale measurements of climatically important atmospheric gases and aerosols, Philosophical Transactions of the Royal Society of London A: Mathematical, Physical and Engineering Sciences 369 (1943) (2011) 2073–2086. arXiv:http://rsta.royalsocietypublishing.org/

content/369/1943/2073.full.pdf, doi:10.1098/rsta.2010.0313.
URL http://rsta.royalsocietypublishing.org/content/369/1943/2073

[24] F. Hilton, R. Armante, T. August, C. Barnet, A. Bouchard, C. Camy-Peyret, V. Capelle, L. Clarisse, C. Clerbaux, P.-F. Coheur, A. Collard, C. Crevoisier, G. Dufour, D. Edwards, F. Faijan, N. Fourri, A. Gambacorta, M. Goldberg, V. Guidard, D. Hurtmans, S. Illingworth, N. Jacquinet-Husson, T. Kerzenmacher, D. Klaes, L. Lavanant, G. Masiello, M. Matricardi, A. McNally, S. Newman, E. Pavelin, S. Payan, E. Pquignot, S. Peyridieu, T. Phulpin, J. Remedios, P. Schlssel, C. Serio, L. Strow, C. Stubenrauch, J. Taylor, D. Tobin, W. Wolf, D. Zhou, Hyperspectral earth observation from iasi: Five years of accomplishments, Bulletin of the American Meteorological Society 93 (3) (2012) 347–370. arXiv:http://dx.doi.org/10.1175/BAMS-D-11-00027.1, doi:10.1175/BAMS-D-11-00027.1.
URL http://dx.doi.org/10.1175/BAMS-D-11-00027.1

[25] U. Amato, L. Lavanant, G. Liuzzi, G. Masiello, C. Serio, R. Stuhlmann, S. Tjemkes, Cloud mask via cumulative discriminant analysis applied to satellite infrared observations: scientific basis and initial evaluation, Atmospheric Measurement Techniques 7 (10) (2014) 3355–3372.

[26] K. Masuda, T. Takashima, Y. Takayama, Emissivity of pure and sea waters for the model sea surface in the infrared window regions, Remote Sensing of Environment 24 (2) (1988) 313 – 329. doi:http://dx.doi.org/10.1016/0034-4257(88)90032-6.
URL http://www.sciencedirect.com/science/article/pii/0034425788900326

[27] C. Serio, C. Standfuss, G. Masiello, G. Liuzzi, E. Dufour, B. Tournier, R. Stuhlmann, S. Tjemkes, P. Antonelli, Infrared atmospheric sounder interferometer radiometric noise assessment from spectral residuals, Appl.

Opt. 54 (19) (2015) 5924–5936. doi:10.1364/AO.54.005924.
URL http://ao.osa.org/abstract.cfm?URI=ao-54-19-5924

[28] U. Amato, G. Masiello, C. Serio, M. Viggiano, The σ-IASI code for the calculation of infrared atmospheric radiance and its derivatives, Environmental Modelling & Software 17 (7) (2002) 651–667.

[29] G. Liuzzi, G. Masiello, C. Serio, D. Meloni, C. Di Biagio, P. Formenti, Consistency of dimensional distributions and refractive indices of desert dust measured over lampedusa with iasi radiances, Atmospheric Measurement Techniques 10 (2) (2017) 599–615. doi:10.5194/amt-10-599-2017.
URL http://www.atmos-meas-tech.net/10/599/2017/

[30] S. Clough, M. Shephard, E. Mlawer, J. Delamere, M. Iacono, K. Cady-Pereira, S. Boukabara, P. Brown, Atmospheric radiative transfer modeling: a summary of the {AER} codes, Journal of Quantitative Spectroscopy and Radiative Transfer 91 (2) (2005) 233 – 244. doi:https://doi.org/10.1016/j.jqsrt.2004.05.058.
URL http://www.sciencedirect.com/science/article/pii/S0022407304002158

[31] A. Carissimo, I. De Feis, C. Serio, The physical retrieval methodology for IASI: the δ-IASI code, Environmental Modelling & Software 20 (9) (2005) 1111–1126.

[32] A. M. Lubrano, G. Masiello, M. Matricardi, C. Serio, V. Cuomo, Retrieving N_2O from nadir-viewing infrared spectrometers, Tellus B 56 (3) (2004) 249–261.

[33] C. D. Rodgers, B. J. Connor, Intercomparison of remote sounding instruments, Journal of Geophysical Research: Atmospheres 108 (D3) (2003) n/a–n/a, 4116. doi:10.1029/2002JD002299.
URL http://dx.doi.org/10.1029/2002JD002299

[34] C. Mennella, Il clima d'italia, EDART, Napoli, Italy.

Spectral Range Number, j	Wavenumber Range cm^{-1}	Number of IASI Spectral Radiances, N_j	Number of Random Components, n_j	Inflation Factor λ_F^2	
				Night	Day
1	645 to 800	621	100	3	3
2	800 to 1210	1640	300	1.5	1.5
3	1210 to 1600	1560	200	10	10
4	1600 to 2000	1600	200	10	10
5	2000 to 2240	960	100	3	3
6	2240 to 2400	640	100	3	500
7	2400 to 2760	1440	200	3	3

Table 1: Definitions of IASI spectral ranges used within the inverse/forward model, number of Random Projections and default values of inflation factors

6. Tables

7. Figures

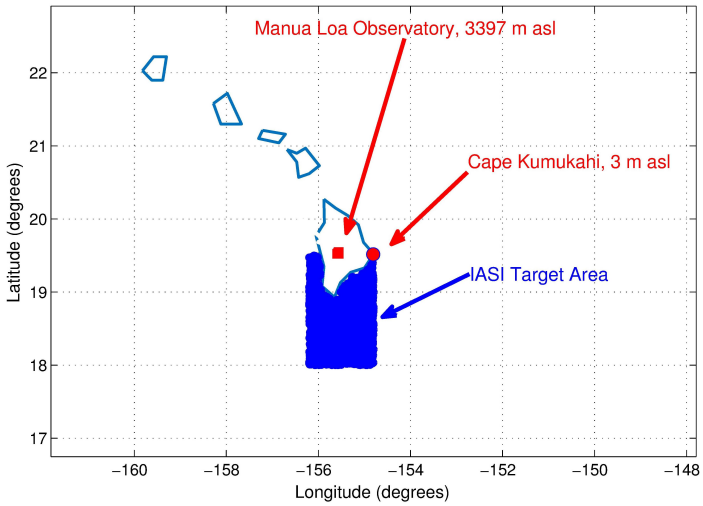

Figure 1: Hawaii case study target area showing the region for which IASI data have been acquired for the period 2014-2015. The figure also shows the location of Mauna Loa and Cape Kumukahi stations.

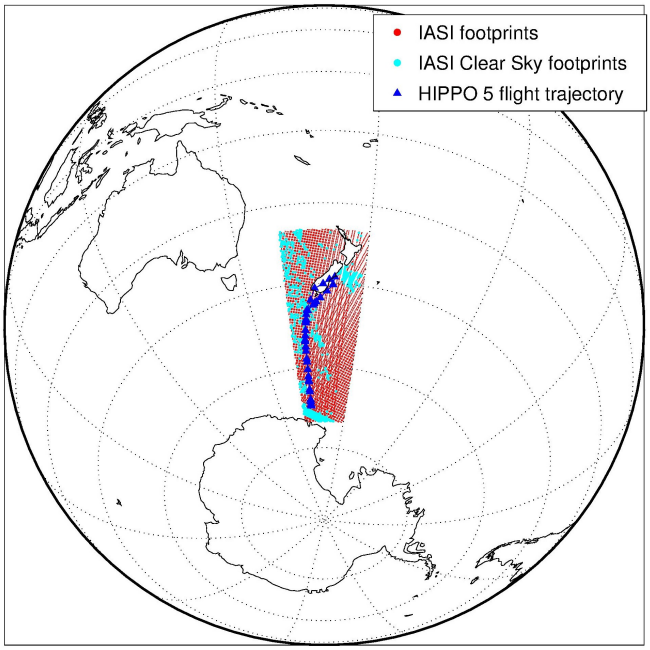

Figure 2: HIPPO5 target area showing the region for which IASI data have been acquired (orbit on 29-Aug-2011, 20:17:28 UTC to 22:07:39 UTC). The HIPPO5 flight trajectory is also shown.

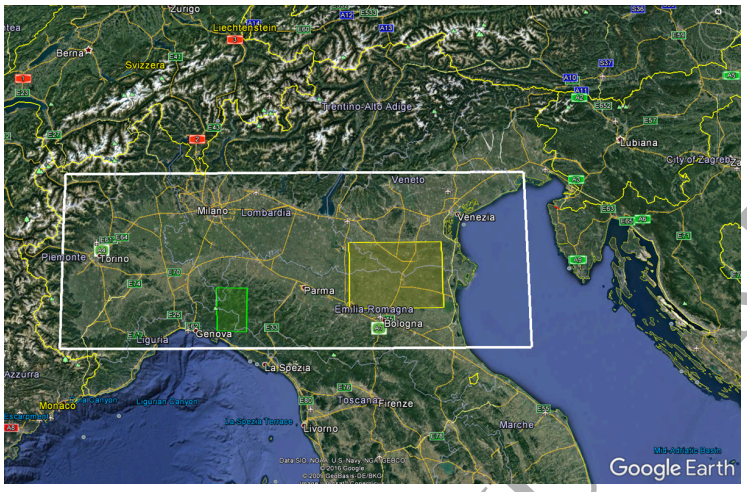

Figure 3: Po Valley (white rectangle) target area. The smaller yellow and green rectangles identify two regions covered mostly by agricultural fields and forest canopy, respectively.

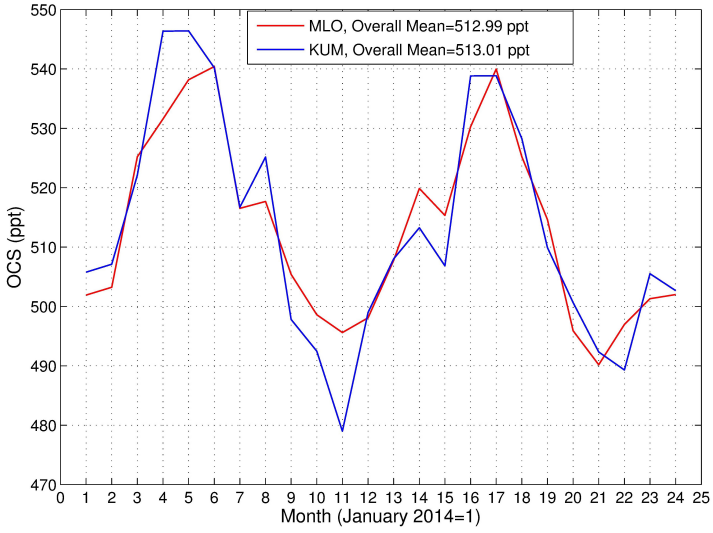

Figure 4: OCS monthly mean for the two surface validation stations, MLO and KUM, which are used for validations of IASI retrievals.

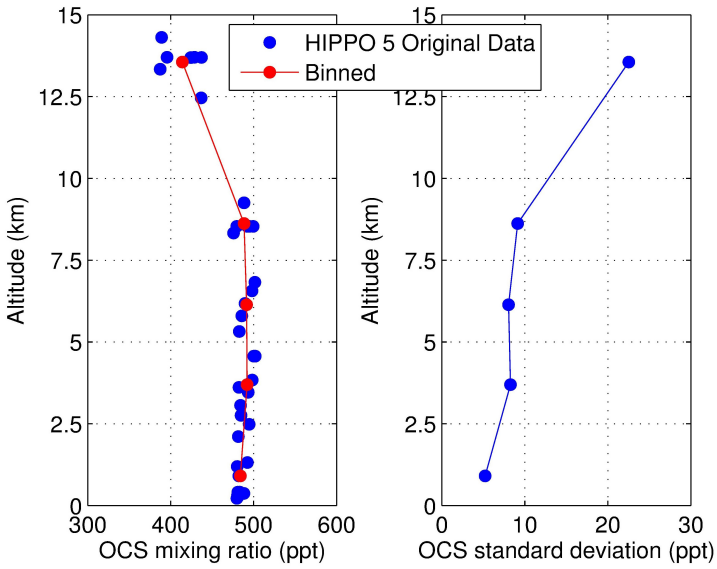

Figure 5: Original HIPPO5 OCS data (left panel) collected over the region shown in 2. The binning shown in figure has been used to derive the standard deviation (right panel)

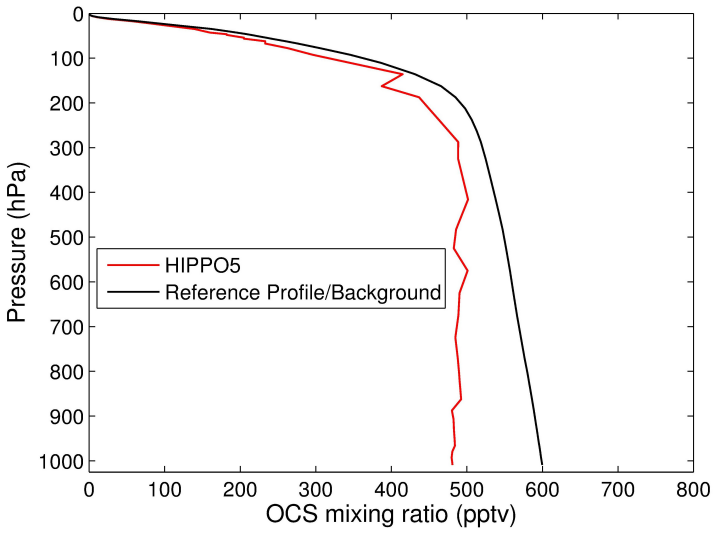

Figure 6: HIPPO5 OCS data interpolated/extrapolated to the forward model pressure layers and comparison with the AFGL reference profile used as a background.

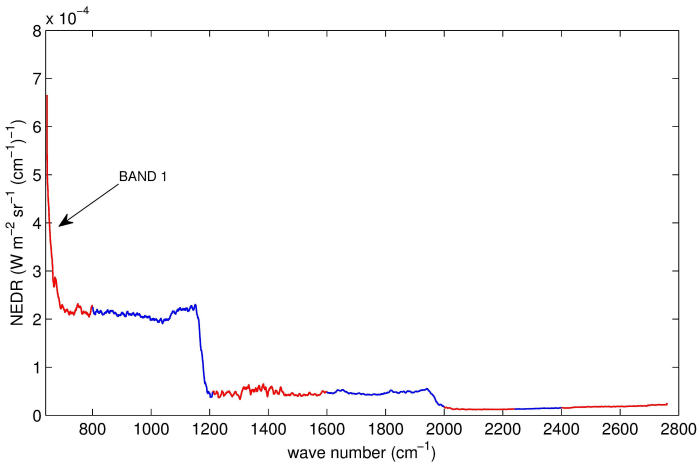

Figure 7: IASI radiometric noise (in Noise Equivalent Difference Radiance (NEDR) units) used in this analysis, after [27]. The plot also shows the wavenumber range of the 7 RP spectral bands defined in Tab. 1: from left, spectral range 1 (red), next spectral range 2 (blue) and further on according to the blue-red sequence.

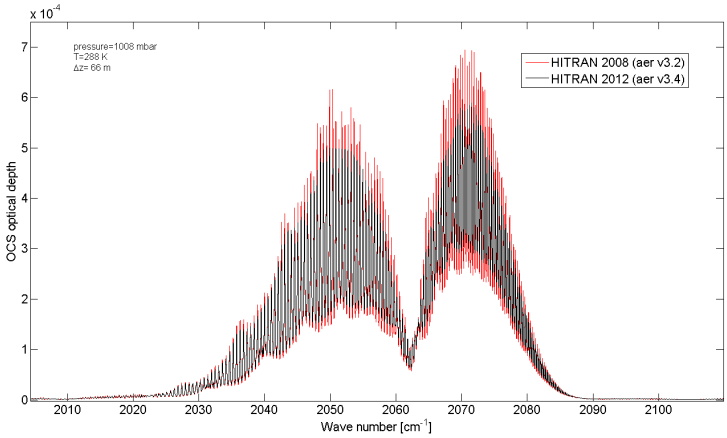

Figure 8: Exemplifying the differences of OCS optical depth between HITRAN2008 and HITRAN2012.

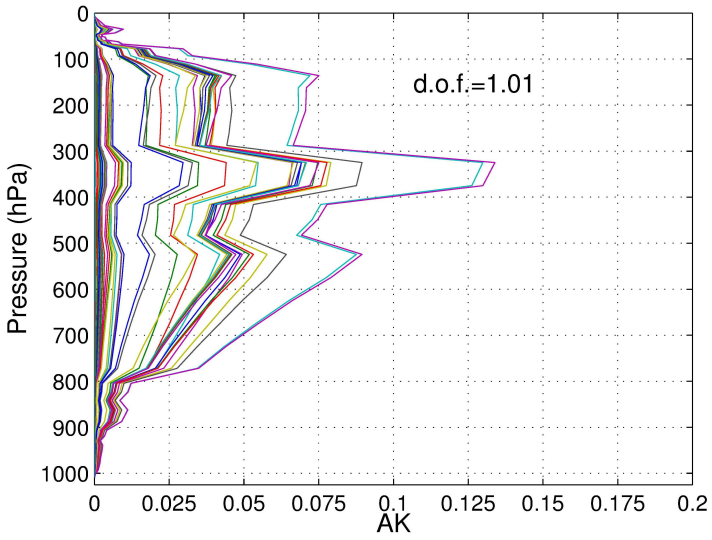

Figure 9: Example of Averaging Kernels for the OCS profile.

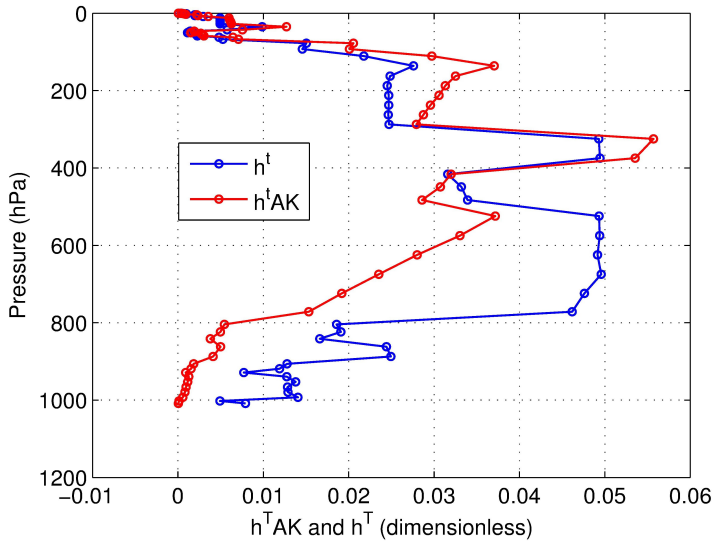

Figure 10: Example of Averaging Kernels for the OCS column retrieval.

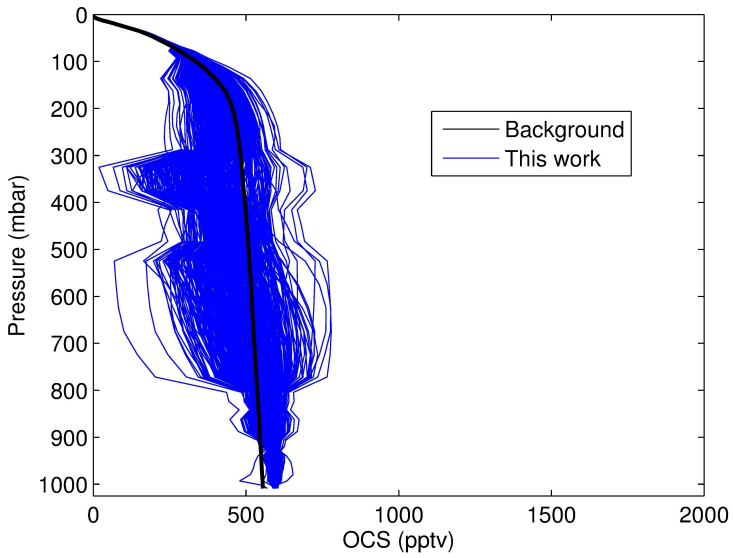

Figure 11: HIPPO5 case study. OCS profiles retrieved over the target area shown in Fig. 2

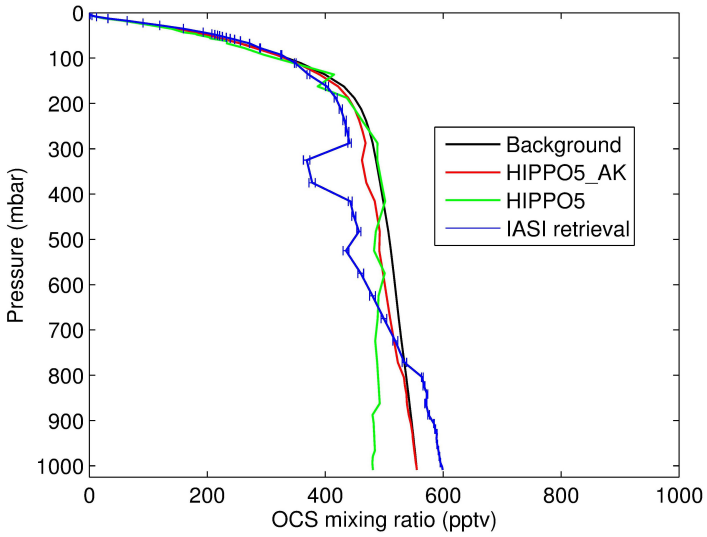

Figure 12: HIPPO5 case study. IASI OCS profile averaged over 415 soundings and comparison with the background, the original HIPPO5 profile and the HIPPO5 (HIPPO5_AK in legend) projected to the IASI retrieval space. The error bar for the retrieval is the standard deviation at each layer based on the 415 soundings divided by the square root of 415.

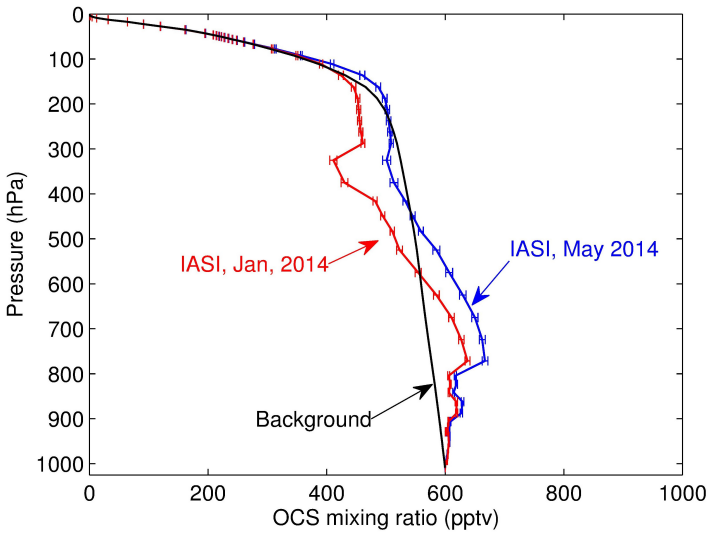

Figure 13: MLO case study. Monthly mean OCS profile for Jan. 2014 and May 2014 derived from IASI night time soundings. The background OCS profile is shown for comparison. Error bars for the retrieved profiles are the standard deviations at each layer divided by the square root of the number of IASI soundings.

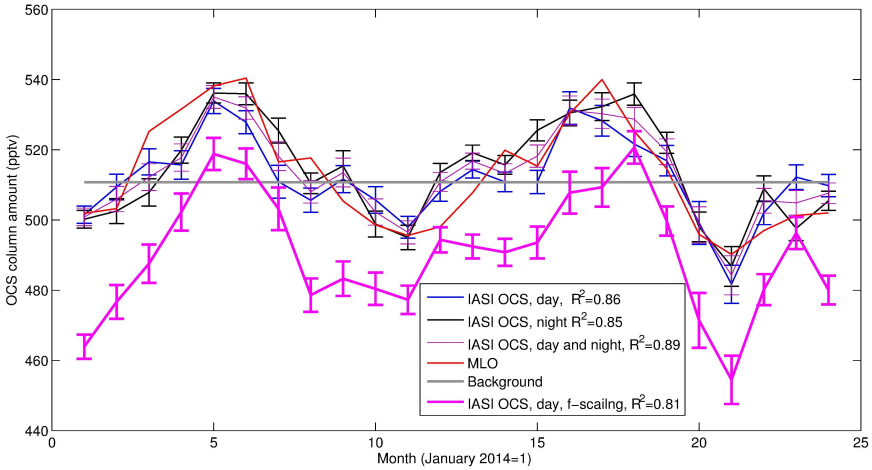

Figure 14: Non-parametric approach. Night-day time and their combination IASI retrieved monthly column averaged mixing ratio (pptv) for OCS and comparison with MLO in situ data. IASI retrievals have been spatially averaged over the target area shown in 1. The error bar represents the error in the mean (standard deviation of soundings in the target area for the given months divided by the square root of the number of observations). R^2 in figure is the linear correlation coefficient of in situ observations against IASI retrieval. Also shown in figure is the day time OCS retrieval for the f-sclaing approach.

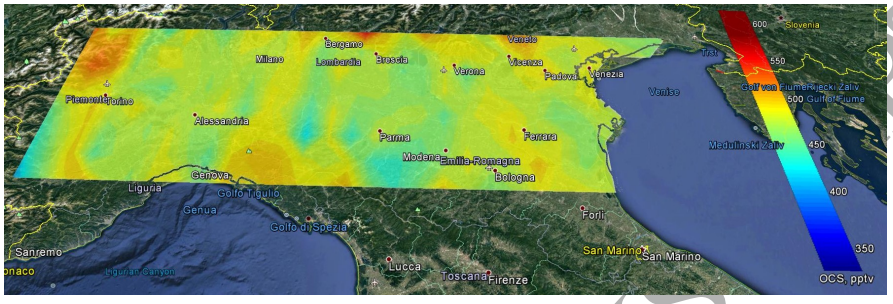

Figure 15: Contour map of monthly mean IASI OCS for February 2015. The IASI retrieval has been smoothed and rendered on a grid of $0.2° \times 0.2°$.

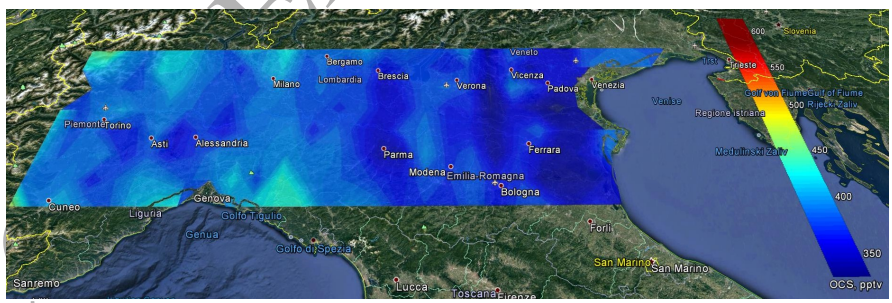

Figure 16: As Fig. 15, but for August 2015.

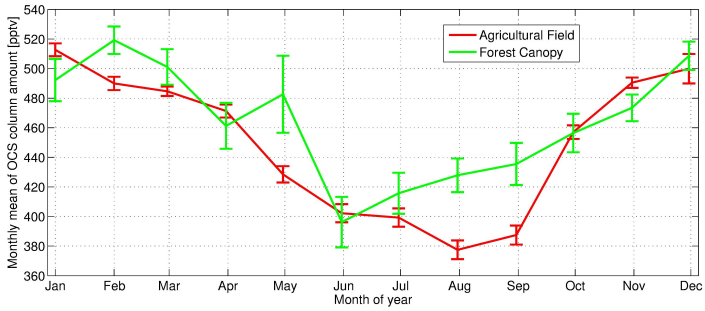

Figure 17: Annual cycle of column mean OCS two regions of the Po Valley: agricultural field (corresponding to yellow rectangle area in Fig. 3) and forest canopy (green rectangle area in Fig. 3). IASI retrievals have been averaged over the area of interest. Error bars are standard deviations divided by the number of data points to form the average value.